J. Fluid Mech. (1990), *vol.* 212, *pp.* 111–137
Printed in Great Britain

Concentration waves in dilute bubble/liquid mixtures

By L. VAN WIJNGAARDEN AND C. KAPTEYN
University Twente, Postbus 217, 7500 AE Enschede, The Netherlands

(Received 15 May 1989)

In this paper we consider a uniform gas bubble–liquid mixture rising under buoyancy. When the gas volume flux is decreased, while keeping bubble size constant, a smooth transition is formed between the region of lower concentration by volume and the region of initial concentration. This transition travels through the mixture as a permanent wave. We start by discussing the mechanisms which make possible such a permanent wave. The first is its tendency to steepen at the low concentration side. At the root of this is the decrease of the uniform rise velocity, under buoyancy, with increasing concentration. Associated with the motion of the bubbles is the liquid impulse. It is shown that this increases with increasing concentration, producing a reactive force on the bubbles which counteracts buoyancy and reduces the force available to overcome friction. In the transition a balance between these two effects occurs. The internal structure following from this balance is analysed in detail and it is shown that under certain conditions all its properties can be derived from knowledge of the average rise velocities of bubbles in uniform mixtures as a function of concentration.

Measurements on these are reported subsequently, followed by a discussion of our experiments on transitions of the kind mentioned in which velocity, thickness etc. of the waves have been measured. The data are compared with the results of the analysis. Order-of-magnitude agreement is found but there are differences as well, requiring further research.

1. Introduction

In a recent paper Batchelor (1988) dealt with the dynamics of waves in fluidized beds. With gas as the fluid, as is the case usually, the particles are heavy and the fluid light. Inertia effects, known as virtual mass effects, are less important. Batchelor (1988) discussed these effects briefly and noted that inertia effects are important in bubbly flows where the particles have almost zero density and the fluid has a large density. In this paper we shall deal with permanent waves in bubbly flow and discuss in particular the effects of the fluid inertia, represented by the added mass of the bubbles. The importance of fluid inertia associated with the motion of the bubbles will be made clear in a qualitative way in this introduction.

Consider, as in figure 1, a uniform suspension of identical bubbles with diameter $2a$ of about 10^{-3} m and rising under buoyancy. The mean velocity of rising results from an equilibrium, on average, between friction and buoyancy. We denote this velocity U_{eq}, to be distinguished later from the average velocity U in a wave where this average velocity is a function of position along the tube. We shall report measurements of U_{eq} in figure 8. These can be represented as, see relation (7.2) below,

$$(U_{eq} - U_0) = V(1 - \lambda\alpha), \tag{1.1}$$

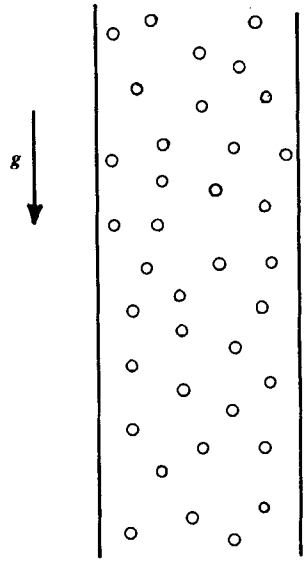

FIGURE 1. A uniform suspension of bubbles in liquid, rising under buoyancy.

where α is the concentration by volume, V and λ are constants and U_0 is the volume flow velocity. In unidirectional flow with liquid velocity U_ℓ, U_0 is defined as

$$U_0 = \alpha U + (1-\alpha)\, U_\ell. \tag{1.2}$$

Two things are worth noting. First $U_{\mathrm{eq}} - U_0$ tends, for $\alpha \to 0$, to a constant, V. This however is not necessarily the velocity with which an isolated bubble rises. We denote the latter U_∞. Experiments show that V is smaller than U_∞. Secondly, U_{eq} becomes smaller with increasing α. This has important consequences for the dynamics of non-uniform phenomena, like the wave represented in figure 2, where the volume concentration increases from the downstream value α_1 to the larger value α_2 upstream.

It is well known that wavelets carrying a disturbance of α travel at a speed near, but slightly less than, U_{eq}. This means that a disturbance at the downstream side always travels faster than those more upstream. This leads to steepening of a wave of the type depicted in figure 2. Without other processes going on at the same time, a permanent wave would be impossible. The mechanisms that work against the steepening in fluidized beds are, in part, also present here. In contrast, however, in bubbly flows, the fluid inertia provides effects that are almost absent in fluidized beds. Associated with the motion of a bubble is a fluid impulse

$$\boldsymbol{h} = \boldsymbol{m}\cdot(\boldsymbol{u} - \boldsymbol{U}_0), \tag{1.3}$$

where $\boldsymbol{m}$, in general a tensor quantity, is the hydrodynamic or added mass, and $\boldsymbol{u} - \boldsymbol{U}_0$ the bubble velocity with respect to the volume velocity $\boldsymbol{U}_0$. The impulse cannot, as is well known, be identified with fluid momentum but its rate of change is a force. The reaction force when the bubble changes its velocity is $-\mathrm{d}/\mathrm{d}t\{\boldsymbol{m}\cdot(\boldsymbol{u} - \boldsymbol{U}_0)\}$. The main ingredients in the force balance are this force, buoyancy and friction. Representing the latter by $\boldsymbol{f}\cdot(\boldsymbol{u} - \boldsymbol{U}_0)$ and buoyancy by $\rho_\ell \boldsymbol{g}\mathscr{V}$, where ρ_ℓ is the liquid density, $\boldsymbol{g}$ is the acceleration due to gravity and $\mathscr{V}$ the volume of a bubble,

$$\mathscr{V} = \tfrac{4}{3}\pi a^3, \tag{1.4}$$

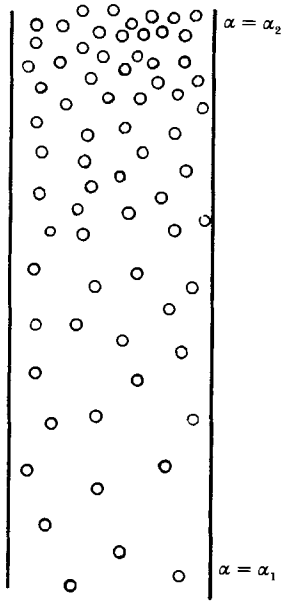

FIGURE 2. A concentration wave in bubbly liquid. The concentration decreases in the wave from an upstream value α_2 to a downstream value α_1.

this balance is
$$\frac{\mathrm{d}}{\mathrm{d}t}\boldsymbol{m}\cdot(\boldsymbol{u}-\boldsymbol{U}_0)+\boldsymbol{f}\cdot(\boldsymbol{u}-\boldsymbol{U}_0)=\rho_\ell \boldsymbol{g}\mathscr{V}. \tag{1.5}$$

The quantity $\boldsymbol{U}_0$ (capital letters express averages, lower case letters values associated with individual bubbles) is the volume flow and consists of an average volume flow of gas $\alpha \boldsymbol{U}$ and, possibly, an average flow of liquid $(1-\alpha)\,\boldsymbol{U}_\ell$. The generalized form of (1.2) is
$$\boldsymbol{U}_0=(1-\alpha)\,\boldsymbol{U}_\ell+\alpha \boldsymbol{U}. \tag{1.6}$$

Since the velocities involved are very small with respect to any velocity of sound, both phases can be considered as incompressible. Then, for a particular flow, $\boldsymbol{U}_0$ is constant. For example, in the uniformly rising suspension in figure 1 $\boldsymbol{U}_0$ equals $\alpha \boldsymbol{U}_{\mathrm{eq}}$. Looking at figure 2, we see that at both extremes there is, on average, equilibrium between friction and buoyancy,
$$\langle \boldsymbol{f}\cdot(\boldsymbol{u}-\boldsymbol{U}_0)\rangle=\rho_\ell \boldsymbol{g}\mathscr{V}. \tag{1.7}$$

Suppose that $\boldsymbol{m}$ in (1.5) is exactly the same as $\boldsymbol{f}$, which would mean that a change of added mass would be accompanied by an equal change in friction coefficient. Then, if there is at the downstream side of a transition as in figure 2 equilibrium between friction force and buoyancy, the solution $\boldsymbol{h}=\rho_\ell \boldsymbol{g}\mathscr{V}$ of (1.5) would remain valid throughout the transition. The impulse associated with the motion of a bubble would remain the same when the bubble travels through an inhomogeneous zone. If, however, $\boldsymbol{m}$ increases more than $\boldsymbol{f}$, with increasing α, and there is near equilibrium, the fluid impulse increases, which acts as a stabilizing, downward, force on the bubble. On the other hand, if $\boldsymbol{m}$ increases less than $\boldsymbol{f}$, the fluid loses impulse. This destabilizes since it acts on the bubbles as an upward force. Indeed, in a study of the

behaviour of waves of small amplitude, van Wijngaarden & Biesheuvel (1988) find that in the absence of Reynolds stresses, stability is guaranteed if

$$\frac{\mathrm{d}}{\mathrm{d}\alpha}\{\langle m_u\rangle/\langle f_u\rangle\} > 0.$$

While the behaviour of $\boldsymbol{m}$ and $\boldsymbol{f}$ is not known in any general sense, some useful insight can be gained for low concentrations. This restriction will be used in the following sections to analyse in more detail what has been said here. Apart from the way in which the average of $\boldsymbol{h}$ behaves, there are also the fluctuations with respect to this average to consider. The fluctuations always provide a stabilizing effect. An order-of-magnitude analysis can be given for low concentrations. It is well known that ensemble averages, such as indicated with angle brackets in (1.7), can be approximated to an accuracy of order α when only pair interactions are taken into account (Batchelor 1972). Since the experiments reported in §7 are all at low α, we shall, after discussion of some aspects of the dynamics of single bubbles, concentrate on the interaction between two bubbles. After that, what has been said above will be worked out in more detail, both from the experimental and the theoretical point of view.

2. Elements of the dynamics of a single bubble

In this section we review some particulars of the flow around a single bubble which we shall need for the analysis of suspensions. We consider bubbles with radius a of the order of 1 mm, rising in water in which the effects of surfactants are negligible.

When dealing with a suspension this condition is more readily met than with a single bubble because in a suspension the available surface-active agents are distributed over a large surface, which makes the concentration on each bubble much smaller than it would be with an isolated bubble. Because there is a boundary layer for the stress but not for the velocity at the surface of the bubble, the velocity distribution can be described by potential theory with an error of $Re^{-\frac{1}{2}}$ where Re is the Reynolds number defined here for velocity u as

$$Re = ua/\nu \tag{2.1}$$

where ν is the kinematic viscosity of the liquid. The shape of the bubble depends on the Weber number We defined as

$$We = 2\rho_\ell u^2 a/\sigma, \tag{2.2}$$

where σ is the coefficient of surface tension. For $We \sim 0$ the bubbles are spherical. For larger We, up to about 4, they assume an oblate spheroidal shape. The flow about a bubble and the associated drag for these conditions have been investigated in two important papers by Moore (1963, 1965). He included in his calculations bubbles deformed by the non-uniform pressure and normal stresses into oblate spheroids. Moore (1965) finds, for the dimensionless drag D,

$$C_D = \frac{D}{\frac{1}{2}\rho u^2 a} = \frac{24}{Re}G(\chi)\left\{1 + \frac{H(\chi)}{Re^{\frac{1}{2}}} + o\left(\frac{1}{Re^{\frac{1}{2}}}\right)\right\}. \tag{2.3}$$

Following Moore, later work has included numerical calculations. Recently Ryskin & Leal (1984) have done computations confirming Moore's analytical results for $We \sim 0$. For higher We they found agreement with Moore's theory to be much worse. In (2.3) χ is the ratio between the long axis and the short axis of the oblate spheroid.

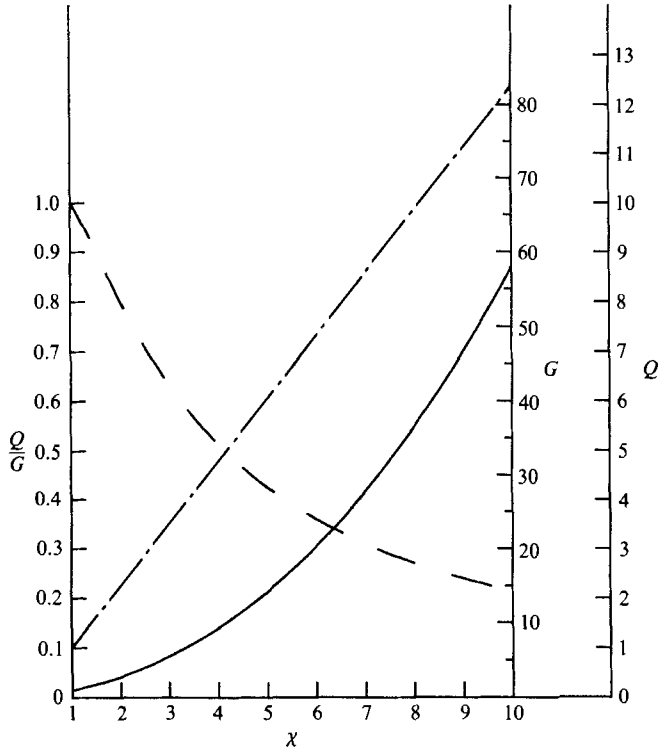

FIGURE 3. The behaviour of $Q(\chi)$, $G(\chi)$ and Q/G as a function of axis ratio χ. ——, $G(\chi)$; —·—·—, $Q(\chi)$; – – – –, Q/G.

$G(\chi)$ and $H(\chi)$ are functions of this axis ratio, given in tabular and in graphic form in Moore (1965). The term involving $H(\chi)$ is true only for steady motion, whereas $G(\chi)$ also holds for unsteady motion since it is connected with the potential part of the flow which is generated instantaneously. With a bubble rising under buoyancy the steady rise velocity is, with $\chi = 1$,

$$U_\infty = ga^2/9\nu \tag{2.4}$$

and the associated Reynolds number is

$$Re \sim a^3/\nu^2.$$

This shows that for a bubble with $a = 1$ mm rising in water, $\nu = 10^{-6}$ m^2/s, $Re \sim 10^3$, which is large enough to make terms with $Re^{-\frac{1}{2}}$ negligible. Comparison with (2.2) shows that such bubbles are already slightly deformed and a more accurate form of (2.4) is

$$U_\infty = ga^2/9\nu G(\chi). \tag{2.5}$$

Figure 3, shows a rapid increase of $G(\chi)$ with χ. Even for bubbles as small as those described here there is a considerable discrepancy between (2.4) and (2.5)† For an isolated bubble rising under gravity the drag force has the direction of the velocity and $\boldsymbol{f}$ in (1.5) is a scalar quantity, f, say. From (2.3) we infer that this has the form

$$f = 12\pi\mu a G(\chi). \tag{2.6}$$

† When measurements of the velocity of rise of single bubbles are interpreted with a view of the applicability of potential flow, this should be borne in mind.

Also, the added mass occurring in (1.5) as $\boldsymbol{m}$ is a scalar quantity for a rising isolated bubble of oblate spheroidal shape.

For a sphere the added mass has the well-known value

$$m_0 = \tfrac{2}{3}\pi\rho a^3. \tag{2.7a}$$

For oblate spheroids the added mass has been given in Milne Thomson (1968, p. 501) as

$$m(\chi) = m_0 Q(\chi), \tag{2.7b}$$

where

$$Q(\chi) = 2\frac{(\chi^2-1)^{\frac{1}{2}} - \cos^{-1}\chi^{-1}}{\cos^{-1}\chi^{-1} - (\chi^2-1)^{\frac{1}{2}}/\chi^2}. \tag{2.8}$$

$Q(\chi)$ is also a function rapidly varying with χ as shown in figure 3. The ratio of m and f plays a crucial role in the present investigation. From (1.5) and (2.6)–(2.8) it follows that a bubble released with velocity U_1 at time $t = 0$ acquires in the course of time a velocity

$$u = U_\infty + (U_1 - U_\infty)\exp(-t/\tau), \tag{2.9}$$

U_∞ being given by (2.5) and with

$$\tau = \frac{a^2}{18\nu}\frac{Q(\chi)}{G(\chi)}. \tag{2.10}$$

τ has the dimension of time and we shall call it the relaxation time because it takes a multiple of τ seconds to bring the initial velocity U_1 down to U_∞. The functions $G(\chi)$ and $Q(\chi)$ together with their ratio Q/G, are given in figure 3.

3. The dynamics of a pair of bubbles

The motion of a bubble in a suspension differs considerably from that of an isolated bubble. Even at small Weber number, where an individual bubble rises along a rectilinear path, bubbles move in a suspension in an erratic way. This is due to the hydrodynamic interaction with other bubbles. The sum of the motion of individual bubbles sets up in the fluid a pressure and stress distribution. This exerts a force on an additional bubble placed in the fluid. This in turn starts to move in such a way that the sum of the forces due to this stress distribution is balanced by the forces due to its own motion and, in addition, buoyancy. Since neighbours change their position continuously the motion of a bubble has a stochastical character. This suggests the use of statistical mechanics, as in other areas of flow of heterogeneous media. As emphasized by Batchelor in his general lecture at Grenoble in 1988 (Batchelor 1989) exact calculations are not likely to go beyond two-particle interactions. For use later on in this paper, we discuss here some aspects of the dynamics of a pair of bubbles.

We refer to figure 4, in which at location $\boldsymbol{x}$ there is a pair of bubbles at mutual distance $2\boldsymbol{R}$ and oriented at an arbitrary angle with respect to $\boldsymbol{g}$. When the bubbles are accelerated, for example by buoyancy, the resulting motion of the centre of mass can be decomposed in two independent directions, along the line of centres and normal to it. Owing to the presence of another bubble, the added mass of the pair is different in both cases. In other words, it is a tensor quantity. Denoting unit vectors

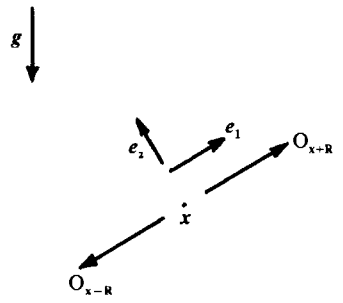

FIGURE 4. A pair of bubbles at distance $2R$, the centre of mass being at location $\boldsymbol{x}$.

along and normal to the line of centres by $\boldsymbol{e}_1$, and $\boldsymbol{e}_2$ respectively, we have from van Wijngaarden (1976), for the added mass of each of two bubbles in a pair:

$$\boldsymbol{m}\cdot\boldsymbol{e}_1 = m_0\left\{1-3\left(\frac{a}{2R}\right)^3+3\left(\frac{a}{2R}\right)^6+9\left(\frac{a}{2R}\right)^8+\ldots\right\}\boldsymbol{e}_1, \tag{3.1}$$

$$\boldsymbol{m}\cdot\boldsymbol{e}_2 = m_0\left\{1+\frac{3}{2}\left(\frac{a}{2R}\right)^3+\frac{3}{4}\left(\frac{a}{2R}\right)^6+3\left(\frac{a}{2R}\right)^8+\ldots\right\}\boldsymbol{e}_2, \tag{3.2}$$

where m_0 is given by $(2.7a)$. These results were obtained by first deriving an expression for the potential due to the motion of two spheres and subsequent calculation of the inertia forces on a bubble, requiring the sum to be zero. The flow potential expressed in coordinates centred in one of the two bubbles can be interpreted as being made up from contributions by a dipole, a quadrupole and higher multipoles. If truncated after the dipole, only the terms in $(a/R)^3$ remain. The same potential can be used to calculate the drag force. This was done by Kok (1988) who extended Moore's (1963) analysis to bubbly suspensions. For a system of bubbles at generalized positions $\boldsymbol{q}_i$ the dissipation function can be formulated.

Using Lagrange's principle, extended with this dissipation function, the equation of motion for each bubble can be derived. We denote by $2\boldsymbol{D}$ the drag force on a pair of bubbles belonging to the motion, with velocity $\dot{\boldsymbol{x}}$ of the centre of mass. In the directions $\boldsymbol{e}_1$ and $\boldsymbol{e}_2$ Kok (1988, 1989) finds

$$\boldsymbol{D}\cdot\boldsymbol{e}_1 = f_0\dot{\boldsymbol{x}}\cdot\boldsymbol{e}_1\left\{1-2\left(\frac{a}{2R}\right)^3+3\left(\frac{a}{2R}\right)^6+11\left(\frac{a}{2R}\right)^8+\ldots\right\}, \tag{3.3}$$

$$\boldsymbol{D}\cdot\boldsymbol{e}_2 = f_0\dot{\boldsymbol{x}}\cdot\boldsymbol{e}_2\left\{1+\left(\frac{a}{2R}\right)^3+\frac{3}{4}\left(\frac{a}{2R}\right)^6+\frac{11}{3}\left(\frac{a}{2R}\right)^8+\ldots\right\}. \tag{3.4}$$

In these relations f_0 is the value of f in (2.6) for $\chi = 1$.

Comparing (3.1) with (3.3) and (3.2) with (3.4) we see that, when we only include terms of order $(a/2R)^3$ we can write

$$\boldsymbol{f} = f_0\{\boldsymbol{I}+\boldsymbol{F}(a/2R)\}, \tag{3.5}$$

$$\boldsymbol{m} = m_0\{\boldsymbol{I}+\tfrac{3}{2}\boldsymbol{F}(a/2R)\}, \tag{3.6}$$

where $\boldsymbol{F}$ has components as given in the curly brackets in (3.3) and (3.4), up to terms of order $(a/R)^6$. In (3.5) and (3.6) $\boldsymbol{I}$ is the unit tensor. These results are not accidental. A fictitious body with added-mass coefficients as given in the right-hand sides of (3.1)

and (3.2) has the same virtual inertia as a spherical bubble when accelerated in the presence of another one at distance $2\boldsymbol{R}$. There is a relation between the impulse $\boldsymbol{h}$ of a body and the dipole strength of a body moving with velocity $\dot{\boldsymbol{x}}$. This relation is (see e.g. Lighthill 1986, p. 136)

$$\boldsymbol{h}+\rho\mathscr{V}\dot{\boldsymbol{x}} = 4\pi\rho_\ell \boldsymbol{d}, \tag{3.7}$$

where $\boldsymbol{d}$ is the dipole strength, that is, the potential of the dipole centred at $\boldsymbol{r} = 0$ is $\varphi = -\boldsymbol{d}\cdot\boldsymbol{r}/r^3$.

Writing the added mass as

$$\boldsymbol{m} = m_0(\boldsymbol{I}+\boldsymbol{L}), \tag{3.8}$$

we have from (3.7) and (3.8)

$$\boldsymbol{d} = \tfrac{1}{2}a^3\dot{\boldsymbol{x}}\cdot(\boldsymbol{I}+\tfrac{1}{3}\boldsymbol{L}). \tag{3.9}$$

The velocity induced by this dipole in a point at distance $\boldsymbol{r} = 2\boldsymbol{R}$ is

$$-\frac{\boldsymbol{d}}{(2R)^3}+3\frac{\boldsymbol{d}\cdot 2\boldsymbol{R}}{(2R)^5}2\boldsymbol{R}.$$

Take for example the aligned case in which $\dot{\boldsymbol{x}}$ is in the direction of $\boldsymbol{R}$. Using (3.9) for $\boldsymbol{d}$ and (3.1) for the appropriate component of $\boldsymbol{L}$, we find for the induced velocity u_{ind} at distance $2\boldsymbol{R}$, in the direction $\dot{\boldsymbol{x}}$,

$$-\frac{2u_{\mathrm{ind}}}{\dot{x}} = -2\left(\frac{a}{2R}\right)^3+2\left(\frac{a}{2R}\right)^6+\ldots = \tfrac{2}{3}(\boldsymbol{L}\cdot\boldsymbol{e}_1)\cdot\boldsymbol{e}_1 \tag{3.10}$$

Next we consider the dissipation. An isolated sphere, moving through the liquid with velocity $\dot{\boldsymbol{x}}$ causes a dissipation

$$\Phi = 12\pi\mu a\,\dot{\boldsymbol{x}}\cdot\dot{\boldsymbol{x}}. \tag{3.11}$$

When there is another sphere in the neighbourhood and only dipoles are taken into account, we may replace the velocity in (3.11) by $\dot{\boldsymbol{x}}+\boldsymbol{u}_{\mathrm{ind}}$, where $\boldsymbol{u}_{\mathrm{ind}}$ is the velocity induced by this neighbour in the centre of the considered sphere. Taking the aligned case, the dissipation function associated with the motion of the pair is twice the quantity

$$\Phi = 12\pi\mu a\,\dot{x}^2\left(1-\frac{u_{\mathrm{ind}}}{\dot{x}}\right)^2 \tag{3.12}$$

(the induced velocity is in the direction of $\dot{x}$). Since the expression in brackets in (3.12) is independent of $\dot{x}$, the drag force $\frac{1}{2}\partial\Phi/\partial\dot{x}$ becomes $12\pi\mu a\,\dot{x}(1-u_{\mathrm{ind}}/\dot{x})^2$.

Expanding this for small $u_{\mathrm{ind}}/\dot{x}$ and using (3.10) gives the first line of (3.3) up to terms of order $(a/2R)^6$ and gives, if we take only the terms in $u_{\mathrm{ind}}/\dot{x}$,

$$12\pi\mu a\,\dot{x}(1+\tfrac{2}{3}(\boldsymbol{L}\cdot\boldsymbol{e}_1)\cdot\boldsymbol{e}_1),$$

giving again the result expressed by (3.5) and (3.6) in the general case. This result ceases to be valid when the bubbles take, for example, the oblate spheroidal shape discussed in §2. For a bubble of such a shape the added mass is already a tensor in the absence of another bubble, $\boldsymbol{M}$, say. The relation between components of $\boldsymbol{L}$ and components of $\boldsymbol{F}$ is therefore different in different directions. Take the position in which the line of centres is perpendicular to $\boldsymbol{g}$. When the centre of mass of the pair is accelerated in the direction of the short principal axis the ratio between the appropriate components of $\boldsymbol{L}$ and $\boldsymbol{F}$ is, within the same approximation as used in deriving (3.5) and (3.6), $\frac{1}{2}(1+\rho_\ell\mathscr{V}/M_{22})$. This is shown in Appendix A. Here $M_{22} = (\boldsymbol{M}\cdot\boldsymbol{e}_2)\cdot\boldsymbol{e}_2$. Similarly the relevant factor is $\frac{1}{2}(1+\rho_\ell\mathscr{V}/M_{11})$ when the centre mass of mass is accelerated in the direction of the long principal axis, see Appendix

A. M_{22} is larger than m_0 by the factor $Q(\chi)$ in (2.8), whereas M_{11} is smaller by a similar factor given by Lamb (1932, §373).

4. Average equations for dilute suspensions

We return to the wave phenomenon as sketched in figure 2. The macroscopic measurable quantities such as void fraction α and velocity $\boldsymbol{U}$ are averages, most conveniently ensemble averages. The ensemble is made up of all possible configurations of N, say, bubbles in a volume large with respect to the inter-bubble distance but small with respect to a macroscopic lengthscale such as, for example, the transition thickness in figure 2. We shall indicate such averages with $\langle\ \rangle$:

$$\langle \boldsymbol{u}-\boldsymbol{U}_0\rangle = (\boldsymbol{U}-\boldsymbol{U}_0). \tag{4.1}$$

In this relation $\boldsymbol{U}$ and $\boldsymbol{u}$ are taken relative to the volume flow $\boldsymbol{U}_0$ as defined in (1.6). In a frame moving with $\boldsymbol{U}_0$ the flow is in general unsteady. In the case of a permanent wave, as in figure 2, there are advantages in considering velocities in a frame moving with the wave velocity $\boldsymbol{U}_s$. In that frame the motion is steady and we have, when z runs along the wave,

$$\frac{\mathrm{d}}{\mathrm{d}z}\alpha(U-U_s) = 0. \tag{4.2}$$

In the wave of figure 2 there is equilbrium at both ends and therefore

$$U_s = \frac{(\alpha U_{eq})_2-(\alpha U_{eq})_1}{\alpha_2-\alpha_1}. \tag{4.3}$$

When $\alpha_2 > \alpha_1$, αU increases with α and, since the total volume flow expressed by U_0 remains constant, (1.6) shows that there is a compensating liquid flow downward. It is readily verified that with equilibrium everywhere, that is $U = U_{eq}$, (4.2) cannot be satisfied and that is where the inertia comes in. Since this includes averages as well as fluctuating quantities we have to go to the particle level. As noted in §1, for dilute suspensions this can be done in terms of interactions between two bubbles. Therefore we give the following discussion in terms of pair interaction. Of course, for higher concentrations multiple interactions have to be considered. This is done in a study by Biesheuvel & Gorissen (1990). Such formulations are more general but at the same time much more complicated. Referring to figure 4 we shall define $P(\boldsymbol{x}-\boldsymbol{R}, \boldsymbol{x}+\boldsymbol{R})\,\mathrm{d}^3\boldsymbol{x}\,\mathrm{d}^3\boldsymbol{R}$ as the probability of finding one bubble in $\boldsymbol{x}-\boldsymbol{R}$ and another one in $\boldsymbol{x}+\boldsymbol{R}$. The quantity P is a probability density, normalized such that, the bubbles being identical,

$$\frac{1}{2}\int P(\boldsymbol{x}-\boldsymbol{R}, \boldsymbol{x}+\boldsymbol{R})\,\mathrm{d}^3\boldsymbol{x}\,\mathrm{d}^3\boldsymbol{R} = \frac{1}{2}\int P(\boldsymbol{x}, \boldsymbol{x}+2\boldsymbol{R})\,\mathrm{d}^3\boldsymbol{x}\,\mathrm{d}^3\boldsymbol{R} = 1.$$

The probability density P obeys a conservation equation

$$\frac{\partial P}{\partial t} + \nabla_{\boldsymbol{x}}\cdot(\boldsymbol{u}P) + \nabla_{\boldsymbol{R}}\cdot(P\dot{\boldsymbol{R}}) = 0, \tag{4.5}$$

where $\boldsymbol{u}$ is, as before, the velocity of the centre of mass of the pair. The relation with the number density $n(\boldsymbol{x})$ can be found by noting that

$$P(\boldsymbol{x}, \boldsymbol{x}+2\boldsymbol{R}) = P(\boldsymbol{x}/\boldsymbol{x}+2\boldsymbol{R})\,P(\boldsymbol{x}+\boldsymbol{R}), \tag{4.6}$$

where $P(\boldsymbol{x}/\boldsymbol{x}+2\boldsymbol{R})$ is the conditional probability density, that is the probability

density of finding a bubble at $\boldsymbol{x}$, given that there is one in $\boldsymbol{x}+2\boldsymbol{R}$. If the one-particle distribution density, $P(\boldsymbol{x})$ or $P(\boldsymbol{x}+2\boldsymbol{R})$, is the same for all $\boldsymbol{R}$ and denoted with the number density $n(\boldsymbol{x})$

$$P(\boldsymbol{x}+2\boldsymbol{R}) = n(\boldsymbol{x}), \tag{4.7}$$

we have, since integration of $P(\boldsymbol{x},\boldsymbol{R})\,\mathrm{d}^3\boldsymbol{R}\,\mathrm{d}^3\boldsymbol{x}$ over all $\boldsymbol{R}$ must give $n(\boldsymbol{x})\,\mathrm{d}^3\boldsymbol{x}$,

$$n(\boldsymbol{x}) = \int P(\boldsymbol{x},\boldsymbol{R})\,\mathrm{d}^3\boldsymbol{R} = \int P(\boldsymbol{x}/\boldsymbol{x}+2\boldsymbol{R})\,P(\boldsymbol{x}+2\boldsymbol{R})\,\mathrm{d}^3\boldsymbol{R}. \tag{4.8}$$

The average $\boldsymbol{U}$ of $\boldsymbol{u}(\boldsymbol{x},\boldsymbol{R})$ now is defined in a similar way:

$$n\boldsymbol{U} = \int P(\boldsymbol{x},\boldsymbol{x}+2\boldsymbol{R})\,\boldsymbol{u}(\boldsymbol{x},\boldsymbol{R})\,\mathrm{d}^3\boldsymbol{R}. \tag{4.9}$$

Thus, integration of the terms in (4.5) over $\boldsymbol{R}$ gives

$$\frac{\partial n}{\partial t} + \nabla_{\boldsymbol{x}}\cdot(\boldsymbol{U}n) = 0. \tag{4.10}$$

Because all bubbles have the same radius a, we obtain, by multiplying this with the volume $\mathscr{V}$ of a bubble,

$$\frac{\partial \alpha}{\partial t} + \nabla_{\boldsymbol{x}}\cdot(\alpha\boldsymbol{U}) = 0. \tag{4.11}$$

This, of course, expresses the conservation of volume flow, which in a frame moving with the wave velocity $\boldsymbol{U}_{\mathrm{s}}$ gives immediately (4.2). Like $\boldsymbol{u}$ other quantities have averages defined in such a way, for example the impulse $\boldsymbol{h}$ of a bubble in the presence of another one at $\boldsymbol{x}+2\boldsymbol{R}$. If we consider $\int \boldsymbol{h}(\boldsymbol{x},\boldsymbol{x}+2\boldsymbol{R})\,P(\boldsymbol{x},\boldsymbol{x}+2\boldsymbol{R})\,\mathrm{d}^3\boldsymbol{R}$ this can be written with the use of (4.6) as

$$\int \boldsymbol{h}(\boldsymbol{x},\boldsymbol{x}+2\boldsymbol{R})\,P(\boldsymbol{x}/\boldsymbol{x}+2\boldsymbol{R})\,P(\boldsymbol{x}+2\boldsymbol{R})\,\mathrm{d}^3\boldsymbol{R} = n\int \boldsymbol{h}(\boldsymbol{x},\boldsymbol{x}+2\boldsymbol{R})\,P(\boldsymbol{x}+2\boldsymbol{R}/\boldsymbol{x})\,\mathrm{d}^3\boldsymbol{R}. \tag{4.12}$$

The integral is precisely the ensemble average accurate in α, provided that the quantity $\boldsymbol{h}$ falls off rapidly enough with increasing R. For example, if we put in (4.12) a constant $\boldsymbol{c}$ instead of $\boldsymbol{h}$ the integral $\int \boldsymbol{c}P(\boldsymbol{x}+2\boldsymbol{R}/\boldsymbol{x})\,\mathrm{d}^3\boldsymbol{R}$ will not exist unless P behaves very specially. The ensemble average of $\boldsymbol{c}$ is of course just $\boldsymbol{c}$, so the reduction is not allowed here, but the ensemble average must be used. In the following we shall be able to deduce the value of averages from experimental results. In those cases where an actual calculation is made we shall take care that integrals like in (4.12) converge.

We turn our attention now to the dynamic equation for the velocity $\boldsymbol{u}-\boldsymbol{U}_0$ of the centre of mass of a pair, relative to the volume velocity $\boldsymbol{U}_0$. This equation is obtained from the equations of motion for the separate bubbles. From addition of these the required equation follows. Incidentally, subtraction gives the equation for the relative motion which is needed when P itself is sought. The pertinent equation for the centre of mass is given in Biesheuvel & van Wijngaarden (1982) and Kok (1988):

$$\frac{\mathrm{d}}{\mathrm{d}t}[\boldsymbol{m}(\boldsymbol{x},\boldsymbol{R},\chi)\cdot\{\boldsymbol{u}-\boldsymbol{U}_0\}] + \boldsymbol{f}(\boldsymbol{x},\boldsymbol{R},\chi)\cdot\{\boldsymbol{u}-\boldsymbol{U}_0\} = \tfrac{4}{3}\pi a^3\boldsymbol{g}\rho_\ell \tag{4.13}$$

The quantities occurring in this equation have all been discussed in previous sections. In the first term on the left-hand side we see the fluid impulse $\boldsymbol{h}$ defined in (1.3). Formally (4.13) is the same as (1.5) but in (4.13) it is understood that in $\boldsymbol{x}$, $\boldsymbol{m}$ and

also $\boldsymbol{f}$ depend only on the presence of another bubble in $\boldsymbol{x}+2\boldsymbol{R}$. We have added χ in the argument as a reminder that the bubbles need not be spherical but are deformed. During the erratic motion of a bubble its shape will change continuously. To take the momentary shape into account in (4.13) would be too complicated. Therefore, we shall consider χ to consist of an average value based on the average rising speed and disregard the fluctuations of the shape. We replace $\boldsymbol{f}$ by $f(\boldsymbol{I}+\boldsymbol{F})$ and $\boldsymbol{m}$ by $m(\boldsymbol{I}+\boldsymbol{L})$, as in (3.5) and (3.8) for the spherical bubble, and use (2.5), (2.6), (2.7) and (2.10) to transform (4.13) to

$$\tau\frac{\mathrm{d}}{\mathrm{d}t}[\{\boldsymbol{I}+\boldsymbol{L}\}\cdot\{\boldsymbol{u}-\boldsymbol{U}_0\}]+\{\boldsymbol{I}+\boldsymbol{F}\}\cdot\{\boldsymbol{u}-\boldsymbol{U}_0\}=\boldsymbol{U}_\infty. \tag{4.14}$$

In the uniformly rising suspension of figure 1, P depends neither on time nor on $\boldsymbol{x}$ and (4.5) reduces for the distribution P_0 to

$$\nabla_{\boldsymbol{R}}\cdot(P_0\dot{\boldsymbol{R}})=0. \tag{4.15}$$

For a uniform suspension all quantities in (4.14) depend only on $\boldsymbol{R}$ and we can write $\mathrm{d}/\mathrm{d}t$ as $\dot{\boldsymbol{R}}\cdot\mathrm{d}/\mathrm{d}\boldsymbol{R}$. We multiply with P_0 and integrate over $\boldsymbol{R}$. Using (4.15), the first term on the left-hand side of (4.14) gives

$$\int\nabla_{\boldsymbol{R}}\cdot[P_0\dot{\boldsymbol{R}}\{(\boldsymbol{I}+\boldsymbol{L})\cdot(\boldsymbol{u}-\boldsymbol{U}_0)\}]\,\mathrm{d}^3\boldsymbol{R}.$$

For fairly general behaviour of the trajectories described by pairs in $\boldsymbol{R}$-space this expression is zero, for example if the trajectories are closed, but also when at the boundaries $\dot{\boldsymbol{R}}$ is zero. Taking therefore the above expression to be zero, the remaining terms in (4.14) give, upon averaging,

$$\langle\{\boldsymbol{I}+\boldsymbol{F}\}\cdot\{\boldsymbol{u}-\boldsymbol{U}_0\}\rangle_{\mathrm{eq}}=\boldsymbol{U}_\infty, \tag{4.16}$$

where the subscript eq is a reminder that the situation is one in which there is, on average, equilibrium between buoyancy and friction. The same result follows, of course, from averaging (4.14) over a long time, following a pair, and using the equivalence between time and ensemble averaging. The relation (4.16) can be written as

$$(\boldsymbol{U}_{\mathrm{eq}}-\boldsymbol{U}_0)=\boldsymbol{U}_\infty-\langle\boldsymbol{F}\cdot(\boldsymbol{u}-\boldsymbol{U}_0)\rangle_{\mathrm{eq}}. \tag{4.17}$$

This says that, with respect to $\boldsymbol{U}_0$, the average rising velocity is the velocity with which an isolated bubble would rise reduced by a term which stems from the average excess resistance over that of an isolated bubble.

Next we turn to the case in which the suspension is not uniform, for example owing to the passage of a wave. In particular we shall consider waves of permanent form travelling with velocity $\boldsymbol{U}_{\mathrm{s}}$. In a frame $\boldsymbol{z}=\boldsymbol{x}-\boldsymbol{U}_{\mathrm{s}}t$ moving with this velocity the flow is steady and we have

$$\nabla_{\boldsymbol{z}}\cdot\{(\boldsymbol{u}-\boldsymbol{U}_{\mathrm{s}})P\}+\nabla_{\boldsymbol{R}}\cdot(P\dot{\boldsymbol{R}})=0. \tag{4.18}$$

Looking at equation (4.14) for the motion of the centre of mass of a pair, $\boldsymbol{u}$ also depends here only on $\boldsymbol{R}$. Hence $\mathrm{d}/\mathrm{d}t$ can be written as $\dot{\boldsymbol{R}}\cdot\mathrm{d}/\mathrm{d}\boldsymbol{R}$. Doing this and multiplying all terms of (4.14) with P, integration over $\boldsymbol{R}$ gives

$$\tau\int P\dot{\boldsymbol{R}}\cdot\nabla_{\boldsymbol{R}}[\{\boldsymbol{I}+\boldsymbol{L}(\boldsymbol{R})\}\cdot\{\boldsymbol{u}-\boldsymbol{U}_0\}]\,\mathrm{d}^3\boldsymbol{R}+\int\{\boldsymbol{I}+\boldsymbol{F}\}\cdot\{\boldsymbol{u}-\boldsymbol{U}_0\}\,(P-P_0)\,\mathrm{d}^3\boldsymbol{R}=0, \tag{4.19}$$

where use has been made of (4.16). The first term on the left-hand side of (4.19) can be worked out, with use of (4.18), as

$$\tau \int P\dot{\boldsymbol{R}}\cdot\boldsymbol{\nabla}_{\boldsymbol{R}}[\{\boldsymbol{I}+\boldsymbol{L}\}\cdot\{\boldsymbol{u}-\boldsymbol{U}_0\}]\,\mathrm{d}^3\boldsymbol{R} = \tau\int \boldsymbol{\nabla}_{\boldsymbol{R}}\cdot[\{\boldsymbol{I}+\boldsymbol{L}\}\cdot\{\boldsymbol{u}-\boldsymbol{U}_0\}P\dot{\boldsymbol{R}}]\,\mathrm{d}^3\boldsymbol{R} + \tau\int[\{\boldsymbol{I}+\boldsymbol{L}\}\cdot\{\boldsymbol{u}-\boldsymbol{U}_0\}]\,\boldsymbol{\nabla}_z\cdot\{P(\boldsymbol{u}-\boldsymbol{U}_s)\}\,\mathrm{d}^3\boldsymbol{R}. \quad (4.20)$$

By the argument which has been used in averaging, in the equilibrium case, the first term in (4.14), we assume that the contribution by the first term on the right-hand side of (4.20) vanishes. The second term can with help of (1.3) and (3.8), which define the impulse $\boldsymbol{h}$, and by using that only P depends on z, which enables $\boldsymbol{\nabla}_z$ to be taken outside the integral, be written as

$$\tau\boldsymbol{\nabla}_z\cdot\int\frac{\boldsymbol{h}}{m_0}(\boldsymbol{u}-\boldsymbol{U}_s)P\,\mathrm{d}^3\boldsymbol{R}. \quad (4.21)$$

The second term on the left-hand side of (4.19) is now written as

$$\int\{\boldsymbol{I}+\boldsymbol{F}(\boldsymbol{R})\}\cdot\{\boldsymbol{u}-\boldsymbol{U}_0\}(P-P_0)\,\mathrm{d}^3\boldsymbol{R} = n\boldsymbol{U}-n\boldsymbol{U}_{\mathrm{eq}}+\int\boldsymbol{F}(\boldsymbol{R})\cdot\{\boldsymbol{u}-\boldsymbol{U}_0\}(P-P_0)\,\mathrm{d}^3\boldsymbol{R}. \quad (4.22)$$

Taking the results expressed by (4.21) and (4.22) together gives

$$n(\boldsymbol{U}-\boldsymbol{U}_{\mathrm{eq}})+\tau\boldsymbol{\nabla}_z\cdot\int\frac{\boldsymbol{h}}{m_0}(\boldsymbol{u}-\boldsymbol{U}_s)P\,\mathrm{d}^3\boldsymbol{R}+\int\boldsymbol{F}(\boldsymbol{R})\cdot\{\boldsymbol{u}-\boldsymbol{U}_0\}(P-P_0)\,\mathrm{d}^3\boldsymbol{R}=0, \quad (4.23)$$

or

$$n\boldsymbol{U} = n\boldsymbol{U}_{\mathrm{eq}}-\int\boldsymbol{F}(\boldsymbol{R})\cdot(\boldsymbol{u}-\boldsymbol{U}_0)(P-P_0)\,\mathrm{d}^3\boldsymbol{R}-\tau\boldsymbol{\nabla}_z\cdot\int\frac{\boldsymbol{h}}{m_0}(\boldsymbol{u}-\boldsymbol{U}_s)P\,\mathrm{d}^3\boldsymbol{R}. \quad (4.24)$$

This result can be interpreted in fluid-mechanical terms in the following way. If we divide by n and multiply with $12\pi\mu aG(\chi)$, (4.24) becomes an average force balance. Clearly, when $P = P_0$ and the suspension is spatially uniform $\boldsymbol{U} = \boldsymbol{U}_{\mathrm{eq}}$ and there is a balance between buoyancy and friction. In the presence of a gradient, the average frictional force $12\pi\mu a\boldsymbol{U}G(\chi)$ differs from that in equilibrium for two reasons. The first is that the probability density distribution is different, P is different from P_0. This makes the part of the frictional force that depends on the presence of others, i.e. $12\pi\mu aG(\chi)\boldsymbol{F}(\boldsymbol{R})\cdot(\boldsymbol{u}-\boldsymbol{U}_0)$, different from the equilibrium value. The second reason is the gradient of the fluid impulse, expressed by the second term on the left-hand side of (4.23). When the fluid impulse increases, the reaction on the bubbles is a downward force reducing the force available to overcome friction. In closing this section, it should be emphasized that at higher concentrations additional forces may be of importance, such as those due to multiple interactions.

5. Waves of permanent form

For waves of permanent form, in which we are primarily interested here, we can simplify (4.23) further. For this we return to the conservation equation (4.18) for P. Since in $\boldsymbol{\nabla}_z\cdot$ only the coordinate z along a wave, such as in figure 2, is concerned,

$$\frac{\partial}{\partial z}(u-U_s)P+\boldsymbol{\nabla}_{\boldsymbol{R}}\cdot(P\dot{\boldsymbol{R}}) = 0. \quad (5.1)$$

The lengthscale for the variation with z is the thickness, d say, of the wave. In $\boldsymbol{R}$-space the bubble radius a is the natural scale. We introduce dimensionless variables

$$\zeta = z/d; \quad \boldsymbol{\eta} = \boldsymbol{R}/a \tag{5.2}$$

in (5.1) to give

$$\frac{a}{d}(u-U_s)\frac{\partial P}{\partial \zeta}+\nabla_{\eta}\cdot(P\dot{\boldsymbol{R}}) = 0.$$

As we shall see when discussing experimental results, the width of the transition is typically of the order of a couple of cm with bubbles of 1 mm radius so that we can put

$$a/d = \epsilon \ll 1, \tag{5.3}$$

which allows to write the above equation as

$$\nabla_{\eta}\cdot(P\dot{\boldsymbol{R}})+\epsilon(u-U_s)\frac{\partial P}{\partial \zeta} = 0. \tag{5.4}$$

This suggests, as in the Enskog method for the solution of the Boltzmann equation in the theory of dilute gases (Chapman & Cowling 1939, chap. 7), expanding the probability density P in a series of ascending powers of ϵ

$$P = P_0+\epsilon P_1+\ldots. \tag{5.5}$$

Inserting (5.3) and (5.5) into (5.4) gives, upon collection of terms of like order in ϵ, the relation (4.15) for P_0, and for the first correction P_1

$$\nabla_{\eta}\cdot(P_1\dot{\boldsymbol{R}}) = -\frac{\partial}{\partial \zeta}\{(u-U_s)P_0\}. \tag{5.6}$$

This equation, together with an additional condition, determines P_1. The additional condition is the following. The integration of $P\,\mathrm{d}^3\boldsymbol{R}\,\mathrm{d}^3\boldsymbol{x}$ over all values of $\boldsymbol{R}$ must give $n(\boldsymbol{x})\,\mathrm{d}^3\boldsymbol{x}$. Requiring now that

$$\int P_0\,\mathrm{d}^3\boldsymbol{R}\,\mathrm{d}^3\boldsymbol{x} = n(\boldsymbol{x})\,\mathrm{d}^3\boldsymbol{x},$$

the condition on P_1 is

$$\int P_1\,\mathrm{d}^3\boldsymbol{R} = 0.$$

This condition and the differential equation for P_1 are sufficient to determine P_1. However, in the present case we do not need to know P_1 explicitly. Taking $\nabla_z\cdot$ equal to $\partial/\partial z$ in (4.24) also and introducing the dimensionless variables, defined in (5.2), in (4.24) gives

$$\boldsymbol{U}-\boldsymbol{U}_{\mathrm{eq}} = \frac{U_\infty\tau}{d}\left[-\frac{\partial}{\partial\zeta}\int\frac{\boldsymbol{h}}{U_\infty m_0}(\boldsymbol{u}-\boldsymbol{U}_s)\frac{P_0a^3}{n}\,\mathrm{d}^3\boldsymbol{\eta}+\frac{a}{U_\infty\tau}\int\left\{\boldsymbol{F}(\boldsymbol{\eta})\cdot(\boldsymbol{u}-\boldsymbol{U}_0)\frac{P_1a^3}{n}\right\}\mathrm{d}^3\boldsymbol{\eta}\right]. \tag{5.7}$$

The magnitude of the parameter $a/U_\infty\tau$, preceding the final term in (5.7), can be deduced from the definitions (2.5) and (2.10) of U_∞ and τ respectively,

$$\frac{a}{U_\infty\tau} = \frac{162\nu^2\{G(\chi)\}^2}{a^3gQ(\chi)}. \tag{5.8}$$

For water, $\nu = 10^{-6}$ m^2/s, and bubbles of about 10^{-3} m radius, this is of order 10^{-2}, whence we neglect the second term with respect to the first in the square brackets on the right-hand side of (5.7).

The quantity $a/U_\infty \tau$ can be interpreted in various ways. One way is to see it as the ratio between the interaction time a/U_∞ and the relaxation time τ. Another is to regard it as a Péclet number with $U_\infty^2 \tau$ as diffusion coefficient. The smallness of this Péclet number means that the balance expressed in (5.7) is mainly maintained by the impulse-flux term. Restoring physical coordinates with the help of (5.2) we have, after this simplification,

$$n\boldsymbol{U} = n\boldsymbol{U}_{\mathrm{eq}} - \tau \boldsymbol{\nabla}_z \cdot \int \frac{\boldsymbol{h}}{m_0} (\boldsymbol{u} - \boldsymbol{U}_{\mathrm{s}}) P_0 \, \mathrm{d}^3\boldsymbol{R}. \tag{5.9}$$

This contains under the integral sign the product of the fluctuating impulse $\boldsymbol{h}$, defined by (1.4) and (3.8), and the fluctuating velocity with respect to $\boldsymbol{U}_{\mathrm{s}}$.

We write

$$n\langle \boldsymbol{h}(\boldsymbol{u} - \boldsymbol{U}_{\mathrm{s}})\rangle = n\langle \boldsymbol{h}\rangle \langle \boldsymbol{u} - \boldsymbol{U}_{\mathrm{s}}\rangle + \int (\boldsymbol{h} - \langle \boldsymbol{h}\rangle)(\boldsymbol{u} - \boldsymbol{U}) P_0 \, \mathrm{d}^3\boldsymbol{R}. \tag{5.10}$$

The average of $\boldsymbol{h}$ can be determined as follows. Using (3.8)

$$\langle \boldsymbol{h}\rangle / m_0 = \langle (\boldsymbol{I} + \boldsymbol{L}) \cdot (\boldsymbol{u} - \boldsymbol{U}_0)\rangle = \langle (\boldsymbol{I} + \boldsymbol{F}) \cdot (\boldsymbol{u} - \boldsymbol{U}_0)\rangle + \langle (\boldsymbol{L} - \boldsymbol{F}) \cdot (\boldsymbol{u} - \boldsymbol{U}_0)\rangle.$$

Since in the pertinent term in (5.7) P_0 is involved we may use (4.16) for the first term on the right-hand side, resulting in

$$\langle \boldsymbol{h}\rangle / m_0 = \boldsymbol{U}_\infty + \langle (\boldsymbol{L} - \boldsymbol{F}) \cdot (\boldsymbol{u} - \boldsymbol{U}_0)\rangle. \tag{5.11}$$

Next we use the relation $\boldsymbol{L} - \boldsymbol{F} = \frac{1}{2}\boldsymbol{F}$ found in §3 to be valid for pairs of spheres to order $(a/R)^3$. As explained at the end of §3, for oblate spheroidal bubbles the ratio between components of $\boldsymbol{L}$ and $\boldsymbol{F}$ is not $\frac{3}{2}$ but different in different directions, sometimes larger, sometimes smaller. In the absence of further knowledge of P_0 we shall assume here that on average we may use the result for spheres. Together with (4.16) this gives for the right-hand side of (5.11)

$$\langle \boldsymbol{h}\rangle / m_0 = \tfrac{3}{2}\boldsymbol{U}_\infty - \tfrac{1}{2}(\boldsymbol{U}_{\mathrm{eq}} - \boldsymbol{U}_0). \tag{5.12}$$

Inserting (5.10) and (5.12) in (5.9), and using the conservation equation (4.2) results in

$$n\boldsymbol{U} = n\boldsymbol{U}_{\mathrm{eq}} - \tfrac{1}{2} n\tau (U_{\mathrm{eq}} - U_{\mathrm{s}}) \frac{\mathrm{d}}{\mathrm{d}z} (\boldsymbol{U}_0 - \boldsymbol{U}_{\mathrm{eq}}) - \tau \boldsymbol{\nabla}_z \cdot \int (\boldsymbol{h} - \langle \boldsymbol{h}\rangle)/m_0 (\boldsymbol{u} - \boldsymbol{U}_{\mathrm{eq}}) P_0 \, \mathrm{d}^3\boldsymbol{R}. \tag{5.13}$$

It is interesting to note that the sign of the average impulse-flux gradient, the second term on the right-hand side of (5.13), depends crucially on the relation between $\boldsymbol{L}$ and $\boldsymbol{F}$. Our experiments as well as those by others show that $U_{\mathrm{eq}} - U_0$ is less than U_∞. This means that in the distribution P_0 the configuration of a pair with the line of centres normal to $\boldsymbol{g}$ has higher probability than the aligned configuration, because in the latter position the resistance is less than the pair would experience when at infinite distance. In the more probable configuration with the line of centres at right angles to the direction of $\boldsymbol{g}$, the excess impulse is, as we have seen in §3, larger than the excess resistance. This results in a stabilizing, downward force on the bubbles, as explained earlier in this paper and confirmed here. At higher concentrations when multiple interactions become important the results of §3 are not accurate enough. It is an interesting subject for future research to investigate whether at higher concentrations the average impulse gradient is negative, which would contribute to the experimentally observed instabilities of voidage waves at high concentrations.

Next we turn to the contribution by the fluctuations to the third term on the right-

hand side of (5.13). With use of (3.8), the average of $(\boldsymbol{h}-\langle\boldsymbol{h}\rangle)/m_0(\boldsymbol{u}-\boldsymbol{U}_{eq})$ can be written as the average of

$$\{(\boldsymbol{I}+\boldsymbol{L})\cdot(\boldsymbol{u}-\boldsymbol{U}_0)-(\boldsymbol{U}-\boldsymbol{U}_0)-\langle\boldsymbol{L}\cdot(\boldsymbol{u}-\boldsymbol{U}_0)\rangle_{eq}\}\{\boldsymbol{u}-\boldsymbol{U}_{eq}\}.$$

This average is equal to

$$\langle(\boldsymbol{u}-\boldsymbol{U})(\boldsymbol{u}-\boldsymbol{U})\rangle+\langle\boldsymbol{L}\cdot(\boldsymbol{u}-\boldsymbol{U}_0)(\boldsymbol{u}-\boldsymbol{U}_{eq})\rangle.$$

It is more convenient to relate $\boldsymbol{u}-\boldsymbol{U}_0$ to $\boldsymbol{U}_\infty$ since at large separation $(\boldsymbol{u}-\boldsymbol{U}_0)$ tends to $\boldsymbol{U}_\infty$. Hence we write the above average as

$$\langle(\boldsymbol{u}-\boldsymbol{U}_0-\boldsymbol{U}_\infty)(\boldsymbol{u}-\boldsymbol{U}_0-\boldsymbol{U}_\infty)\rangle-\{\boldsymbol{U}_\infty-(\boldsymbol{U}_{eq}-\boldsymbol{U}_0)\}\{\boldsymbol{U}_\infty-(\boldsymbol{U}_{eq}-\boldsymbol{U}_0)\}$$
$$+\langle\boldsymbol{L}\cdot(\boldsymbol{u}-\boldsymbol{U}_0)(\boldsymbol{u}-\boldsymbol{U}_0-\boldsymbol{U}_\infty)\rangle+\langle\boldsymbol{L}\cdot(\boldsymbol{u}-\boldsymbol{U}_0)(\boldsymbol{U}_\infty-\boldsymbol{U}_{eq}+\boldsymbol{U}_0)\rangle. \quad (5.14)$$

Using (4.17) and the relation $\boldsymbol{L}=\frac{3}{2}\boldsymbol{F}$ the last term can be written as

$$\tfrac{3}{2}\{\boldsymbol{U}_\infty-(\boldsymbol{U}_{eq}-\boldsymbol{U}_0)\}\{\boldsymbol{U}_\infty-(\boldsymbol{U}_{eq}-\boldsymbol{U}_0)\} \quad (5.15)$$

The last but one term is reduced to

$$\langle\boldsymbol{L}\cdot(\boldsymbol{u}-\boldsymbol{U}_0)(\boldsymbol{u}-\boldsymbol{U}_0-\boldsymbol{U}_\infty)\rangle=\langle\boldsymbol{L}\cdot(\boldsymbol{u}-\boldsymbol{U}_0-\boldsymbol{U}_\infty)(\boldsymbol{u}-\boldsymbol{U}_0-\boldsymbol{U}_\infty)\rangle$$
$$+\langle\boldsymbol{L}\cdot\boldsymbol{U}_\infty(\boldsymbol{u}-\boldsymbol{U}_0-\boldsymbol{U}_\infty)\rangle. \quad (5.16)$$

Inserting (5.15) and (5.16) into (5.14) and using this for evaluating the average of $(\boldsymbol{h}-\langle\boldsymbol{h}\rangle)(\boldsymbol{u}-\boldsymbol{U}_{eq})$ in (5.13) we finally obtain from (5.13)

$$n\boldsymbol{U}=n\boldsymbol{U}_{eq}-\tfrac{1}{2}n\tau(U_{eq}-U_s)\frac{d}{dz}(\boldsymbol{U}_0-\boldsymbol{U}_{eq})-\tfrac{1}{2}n\tau\nabla_z\cdot\{\boldsymbol{U}_\infty-(\boldsymbol{U}_{eq}-\boldsymbol{U}_0)\}$$
$$\{\boldsymbol{U}_\infty-(\boldsymbol{U}_{eq}-\boldsymbol{U}_0)\}-\tau\nabla_z\cdot\int\{(\boldsymbol{I}+\boldsymbol{L})\cdot(\boldsymbol{u}-\boldsymbol{U}_0-\boldsymbol{U}_\infty)$$
$$(\boldsymbol{u}-\boldsymbol{U}_0-\boldsymbol{U}_\infty)\}P_0\,d^3\boldsymbol{R}-\tau\nabla_z\cdot\int\{\boldsymbol{L}\cdot\boldsymbol{U}_\infty(\boldsymbol{u}-\boldsymbol{U}_0-\boldsymbol{U}_\infty)\}P_0\,d^3\boldsymbol{R}. \quad (5.17)$$

The terms with the integrals in (5.17) cannot be inferred from experimentally obtained values for $U_{eq}-U_0$. They are however, in the applications that we shall deal with, considerably smaller than the other terms. The latter can be evaluated as follows. From (4.3) and (1.1) we have

$$U_{eq}-U_s=\lambda V\{\alpha_1+\alpha_2-\alpha\}, \quad (5.18)$$

where we recall that α_1 and α_2 are the downstream and upstream values of α, respectively. The z-component of the third-term on the right-hand side of (5.17) becomes

$$-\tfrac{1}{2}n\tau\frac{d}{dz}\{U_\infty-V(1-\lambda\alpha)\}^2=-n\tau\lambda V\frac{d\alpha}{dz}(U_\infty-V+\lambda V\alpha). \quad (5.19)$$

To estimate the contribution by the integrals in (5.17) we observe that inspection of (4.14) shows that for $\tau\to\infty$ $(\boldsymbol{I}+\boldsymbol{L})\cdot(\boldsymbol{u}-\boldsymbol{U}_0)\to\text{const.}$

Taking the constant equal to $\boldsymbol{U}_\infty$, that is the value that $\boldsymbol{u}-\boldsymbol{U}_0$ approaches for $R\to\infty$, we have

$$\boldsymbol{u}-\boldsymbol{U}_0-\boldsymbol{U}_\infty\sim-\boldsymbol{L}\cdot\boldsymbol{U}_\infty \quad \text{for} \quad \tau\gg1, \quad (5.20)$$

Similarly

$$\boldsymbol{u}-\boldsymbol{U}_0-\boldsymbol{U}_\infty\sim-\boldsymbol{F}\cdot\boldsymbol{U}_\infty \quad \text{for} \quad \tau\ll1. \quad (5.21)$$

Since the elements of $\boldsymbol{L}$ and $\boldsymbol{F}$ decrease like $(a/R)^3$ we may apply (4.12) and the discussion it follows to both integrals in (5.17), for the particular case of $\boldsymbol{h}$. We take

$P_0(\boldsymbol{x}/\boldsymbol{x}+2\boldsymbol{R})$ to be zero when $R \leqslant a$ and n for $R > a$. Then, using (4.12) we find for the sum of the terms with integrals in (5.17), when (5.20) is used,

$$\frac{\mathrm{d}}{\mathrm{d}z}\left\{-\tau n^2 U_\infty^2 \int_a^\infty \left(\frac{a^3}{8R^3}\right)^3 4\pi R^2 \,\mathrm{d}R\right\} = -0.001 n\tau U_\infty^2 \frac{\mathrm{d}\alpha}{\mathrm{d}z} \tag{5.22}$$

and, when (5.21) is used,

$$\frac{\mathrm{d}}{\mathrm{d}z}\left[-\tau n^2 U_\infty^2 \int \left\{\frac{3}{2}\left(\frac{a^3}{8R^3}\right)^3 - \frac{1}{2}\left(\frac{a^3}{8R^3}\right)^2\right\} 4\pi R^2 \,\mathrm{d}R\right] = 0.006 n\tau U_\infty^2 \frac{\mathrm{d}\alpha}{\mathrm{d}z}. \tag{5.23}$$

Since in our experiments α is of the order of 10% it seems that, concerning the estimates in (5.22) and (5.23), the contributions from the other terms, of which one is given in (5.19) and the other follows from (1.1) and (5.18), are much larger. Then, neglecting the terms with the integrals in (5.17), introducing (5.18) and (5.19) in (5.17) gives upon division by n

$$U_{\mathrm{eq}} - U = \tfrac{1}{2}\tau\lambda^2 V^2 \frac{\mathrm{d}\alpha}{\mathrm{d}z}\left\{(\alpha_1+\alpha_2+\alpha) + 2\frac{U_\infty - V}{\lambda V}\right\}. \tag{5.24}$$

An equation for α is obtained by writing the left-hand side of (5.24) as $(U_{\mathrm{eq}}-U_{\mathrm{s}})+(U_{\mathrm{s}}-U)$ and using (5.18) for the former term, while using for the latter the relation, following from (1.1), (4.2) and (4.3),

$$U - U_{\mathrm{s}} = \frac{\alpha(U-U_{\mathrm{s}})}{\alpha} = \frac{\{\alpha(U-U_{\mathrm{s}})\}_1}{\alpha} = \frac{\alpha_1\alpha_2\lambda V}{\alpha}.$$

With this we obtain as final result the equation

$$(\alpha-\alpha_1)(\alpha_2-\alpha) = \tfrac{1}{2}\alpha\tau\lambda V \frac{\mathrm{d}\alpha}{\mathrm{d}z}\left(\alpha_1+\alpha_2+\alpha+2\frac{U_\infty - V}{\lambda V}\right). \tag{5.25}$$

The right-hand side of (5.24) may be interpreted as a diffusional flux with diffusion coefficient

$$\mathscr{D} = \tfrac{1}{2}\tau(\lambda V)^2\left(\alpha_1+\alpha_2+2\frac{U_\infty - V}{\lambda V}\right) \tag{5.26}$$

or, with

$$q = \tfrac{1}{2}\left(\alpha_1+\alpha_2+2\frac{U_\infty - V}{\lambda V}\right), \tag{5.27}$$

$$\mathscr{D} = q\tau(\lambda V)^2. \tag{5.28}$$

Solution of (5.25) gives, allowing for a constant, z_0,

$$\frac{(\alpha-\alpha_1)^{\alpha_1(1+\alpha_1/2q)}}{(\alpha_2-\alpha)^{\alpha_2(1+\alpha_2/2q)}} \exp -\{\alpha(\alpha_2-\alpha_1)/2q\} = \exp \frac{\lambda V(z-z_0)(\alpha_2-\alpha_1)}{\mathscr{D}}. \tag{5.29}$$

It follows that $\alpha \to \alpha_1$ for $z \to -\infty$ and $\alpha \to \alpha_2$ for $z \to \infty$. In these far regions of the transition we have

$$\alpha - \alpha_1 \sim \exp\left\{\frac{\lambda V(z-z_0)(\alpha_2/\alpha_1 - 1)}{\mathscr{D}(1+\alpha_1/2q)}\right\} \qquad (\alpha \to \alpha_1), \tag{5.30}$$

$$\alpha_2 - \alpha \sim \exp -\left\{\frac{\lambda V(z-z_0)(1-\alpha_1/\alpha_2)}{\mathscr{D}(1+\alpha_2/2q)}\right\} \quad (\alpha \to \alpha_2). \tag{5.31}$$

Since $\alpha_2 > \alpha_1$ we see that (5.29) predicts a steeper transition at the downstream side,

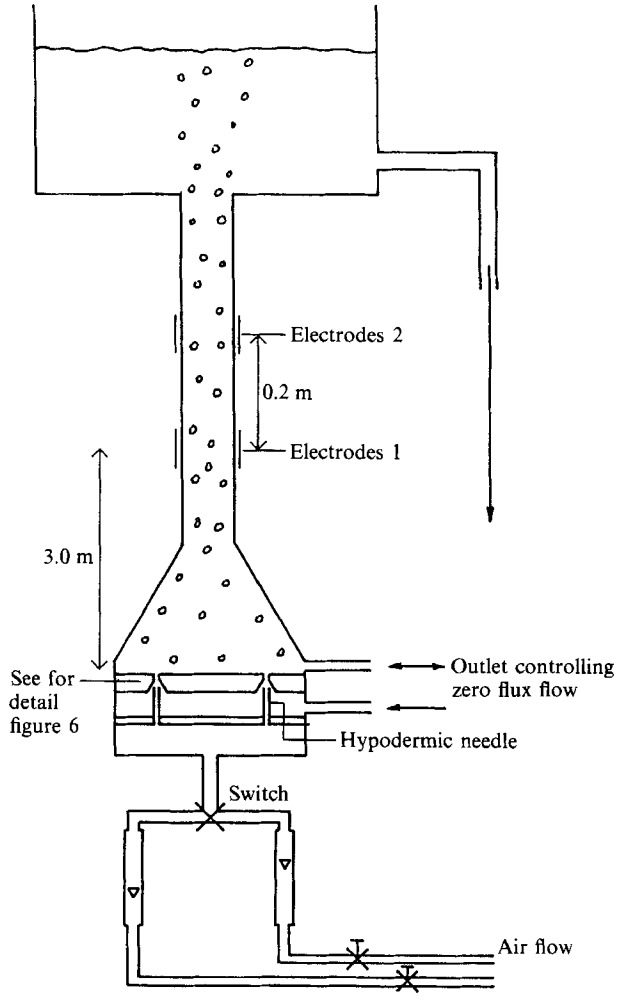

FIGURE 5. A sketch of the experimental set-up.

where $\alpha \to \alpha_1$, than at the upstream side where $\alpha \to \alpha_2$. Further it can be seen that the thickness of the transition, d, is a multiple of

$$\frac{\mathscr{D}}{\lambda V}\left\{\frac{1+\alpha_1/2q}{\alpha_2/\alpha_1-1}+\frac{1+\alpha_2/2q}{1-\alpha_1/\alpha_2}\right\}=\frac{\mathscr{D}}{\lambda V}\left\{\frac{\alpha_2+\alpha_1+(\alpha_1^2+\alpha_2^2)/2q}{\alpha_2-\alpha_1}\right\}. \tag{5.32}$$

6. Description of the experiments

In order to verify the analysis given in the preceding sections, experiments have been carried out on a water/air-bubble mixture in a vertical duct. Essential conditions on the two-phase mixture are a small variation in bubble size and not too large bubbles, otherwise the bubble deformation becomes too large for the theory to be valid. Basically the experimental set-up is an open water loop consisting of two horizontal and two vertical ducts. A sketch is given in figure 5. The vertical mixture duct has a circular cross-section of 8 cm internal diameter. At the bottom of the mixture duct a bubble generator is mounted, which injects the air bubbles into the

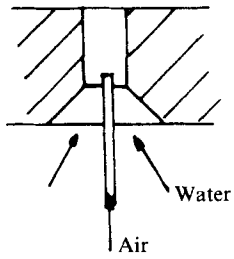

FIGURE 6. A hypodermic needle and the water channel outside it to modify the bubble size.

system, while an open tank at the top of the set-up enables the air bubbles to escape. Special attention has been paid to the bubble production. The air is injected through 150 hypodermic needles of 0.5 mm internal diameter. These needles can operate in two modes. At low volume fluxes of air a needle produces air bubbles one by one, while at high air flow rates an air jet emerges from the needle, which breaks up into bubbles above the needle tip. The latter situation is less suitable, as the variation in the bubble diameter is large. To enlarge the region in which the first mode occurs and at the same time to enable the adjustment of the bubble dimensions, each needle is positioned in a narrow water channel. When the water flow through the channel is increased then, owing to the larger forces between water flow and growing bubbles, smaller bubbles are released. A more detailed picture of this bubble-producing device is given in figure 6. The production of bubbles is accompanied by a flow of water. The net water flow upward in the duct has to be controlled independently. To achieve a prescribed water flow (zero in the experiments to be described) there is an outlet enabling a prescribed net volume flow of water.

Void fraction can be measured with one of the following devices: (1) a Betz pressure difference meter (volume- and time-averaged data); (2) an electric conductance system with electrodes mounted flush with the wall (volume-averaged data); (3) a measurement system based on gamma photon absorption (local- and volume-averaged data). Methods 2 and 3 are also suited for measuring the propagation speed of void-fraction disturbance in the axial direction, when the time delay between the passage past two measurement positions at a certain distance from each other is determined.

The volume of the bubbles produced is obtained by leading individual bubbles out of the two-phase mixture, stretching them into a cylindrical shape, the dimensions of which can be derived after passage past two optical sensors. Mass fluxes of water and air are measured with rotameters.

Since measurements to be reported in §7 have all been done with methods 1 and 2, we give hereafter some details of 2, the operation of Betz pressure difference meters being sufficiently well known. The two-phase mixture between two electrodes mounted flush with the duct wall forms one of the four electric resistances of a Wheatstone bridge. The dimension of the electrodes in the axial direction is 15 mm, which is still sufficiently large with respect to the bubble diameter to prevent too much influence of one single bubble on the imbalance of the bridge. To reduce the influence of the mixture outside the region between the electrodes, 'guard electrodes' have been mounted above and below the 'sensor electrodes', which are all operated at the same voltage.† A picture of the layout of the electrodes is shown in figure 7.

† For the idea of introducing these extra 'guard electrodes' we are indebted to Dr J. Bouré of the Centre d'Etudes Nucleaires de Grenoble.

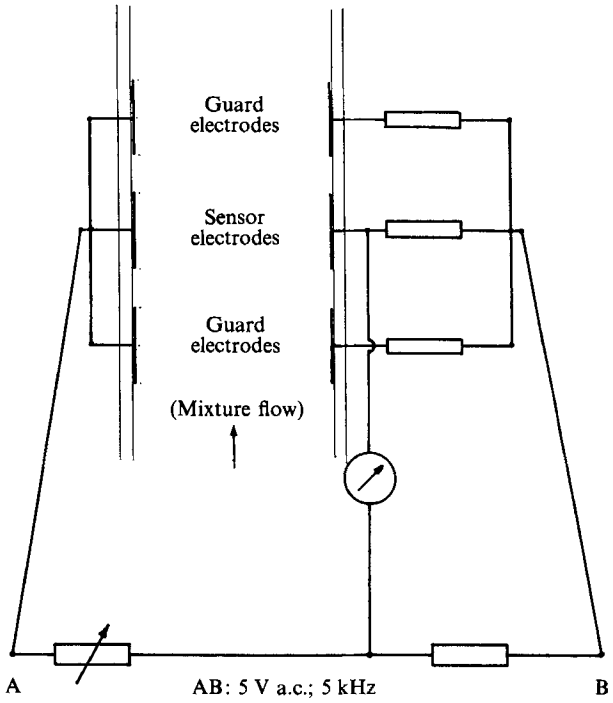

FIGURE 7. An outline of the electric conductance system.

A calibration of this device was carried out, in which the readout of the bridge was compared with the void fraction obtained from the Betz pressure difference meter for the case of uniform mixture conditions in stagnant water. This calibration shows that a nearly linear relation exists between the bridge imbalance and the volume-averaged void fraction under the above-mentioned conditions. For slow variations of α in the axial direction this calibration can be used. To inspect the influence of the finite width of the electrodes, we carried out the following experiment. We took, instead of a bubbly flow, a packed bed of finite length consisting of 5% volume concentration of polystyrene spheres with a diameter of 3 mm. The transition from void to the packed bed was registered by the electrodes as being of finite width of about 1 cm. The concentration behaves as

$$\alpha \sim \tfrac{1}{2}\Delta\alpha\{1+\tanh(sx)\}, \quad s = 115\ \mathrm{m}^{-1}. \tag{6.1}$$

Next we investigated the effect of this on an input

$$\alpha \sim \tfrac{1}{2}\Delta\alpha\{1+\tanh(\lambda x)\}, \quad \lambda < s. \tag{6.2}$$

It appears (see Appendix B) that the relative error is smaller than

$$\tfrac{1}{3}(\lambda/s)^2/\cosh^2(\lambda x), \tag{6.3}$$

which means 8% in the worst case. Hence we have used the calibration without further correction to determine the α-profile in our measured waves.

For completeness we should also briefly describe method 3, gamma absorption, even though results from it are not used in §7. An ^{241}Am source emits a beam of 60 keV photons through the mixture duct. The photon intensity at the other side of the duct is counted by an NaI scintillator/photomultiplier. The number of photons

absorbed is related to the void fraction and after calibration this absorption can be used to measure local or average (over a cross-section) void fraction. The number of photons detected by the scintillator during the passage of a void-fraction transition is rather low, owing to the admitted source strength. Therefore this method has been mainly used for measurements under steady conditions.

The mean bubble rise velocity in a stationary two-phase mixture can be deduced from $U_{eq} = \Phi_g/\alpha A \rho_g$, where Φ_g is the air mass flow, A is the cross-section of the duct and ρ_g is the air density. At the same time the equivalent mean radius of the air bubbles was obtained from the bubble volume measurements. A summation of 25 registrations of void transitions has been made to exclude stochastical variations in the registered profile. To achieve this the experiments were controlled by two coupled computers. One of these, a PDP-11, equipped with analog/digital and counting facilities, counted time intervals, needed for the two-phase mixture in the duct to become stable at the initial void fraction α_2, and also controlled the switching of the air mass flow to the value corresponding with α_1. The other computer, an Olivetti M24 controlled a digital memory oscilloscope, used for the registration of the electrode signals. A 25 Hz low-pass filter was applied in order to suppress high-frequency fluctuations, which could disturb the triggering of the signal. This trigger pulse initializes the measurement on the oscilloscope in such a way that data of the complete wave are registered. Two pairs of electrodes, at a distance of 20 cm were used to determine both the shape and the speed of the waves. Two points have to be taken into account carefully: (i) The position of the trigger point has to be chosen in a region of large void-fraction gradient to diminish effects of small variations in the void-fraction registration on the mean-shock profile. We took the point $\alpha = \frac{1}{2}(\alpha_1 + \alpha_2)$. (ii) The distance between the first electrode pair (trigger source) and the other detectors should not be too large to avoid effects of small velocity differences among succeeding transitions. It appeared that 20 cm is a good choice.

7. Experimental results

The liquid used in the experiments is filtrated tap water. Bubbles have an effective radius of 1.4 mm with a spread of 0.25 mm. For a bubble with an effective diameter of 3 mm Clift, Grace & Weber (1978) report a velocity of rise of 28 cm/s in pure water and 18 cm/s in contaminated water. We have measured

$$U_\infty = 27 \times 10^{-2} \text{ m/s}, \tag{7.1}$$

which is very close indeed to the value in pure water. Our experiments on uniformly rising suspensions give

$$U_{eq} - U_0 = 0.223(1 - 1.78\alpha) \quad (0.02 < \alpha < 0.14). \tag{7.2}$$

A representation of experimental points together with (7.2) is shown in figure 8. The experimental points are, down to concentrations of about 2%, very close to the line given by (7.2). In the interval between $\alpha = 0$ and $\alpha \sim 0.02$ there is scatter and rise velocities are difficult to obtain. This explains why there is a difference between U_∞ in (7.1) and the quantity V in (7.2) (see (1.1)), which therefore should be considered as an empirical quantity rather than the rise velocity for $\alpha \to 0$. Since in our experiments to be reported presently no concentrations below 2% occur we shall use (7.2) in our calculations. In the literature, while data for rise velocities of bubbly

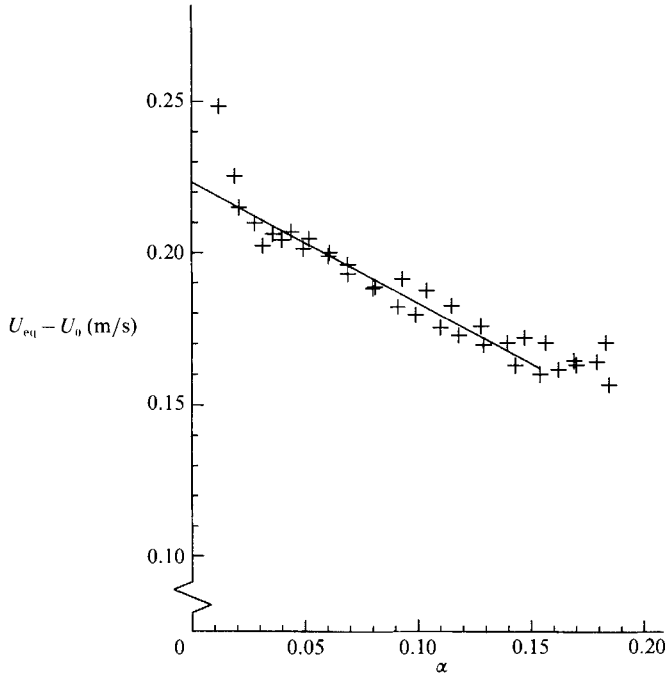

FIGURE 8. $U_{eq} - U_0$ obtained from experiments and the linear relation (7.2) drawn through these points.

suspensions are given, usually there is no specification of bubble size and spread of bubble size. Hetsroni (1982, pp. 2–87) reports

$$U_{eq} - U_0 = U_\infty (1-\alpha)^n \quad (1.75 < n < 2,2). \tag{7.3}$$

Bouré (1988) reports for the suspensions that he and his coworkers have studied

$$U_{eq} - U_0 = 0.22(1-2.25\alpha) + O(\alpha^2). \tag{7.4}$$

Both (7.3) and (7.4) are not very far from our result (7.2), the value 0.22 for V corresponds with what Bouré (1988) finds, whereas the index regime in (7.3) comprises, for $n = 1.78$ and to order α, our result. We consider the latter as more precise since the bubbles in our experiments are of known size with small spread.

An important quantity is the relaxation time τ. This has been calculated as follows. For bubble radius $a = 1.5 \times 10^{-3}$ m and U_∞ as given in (7.1) the Weber number (defined in (2.2)) is 3.1. From Moore (1965) we find $\chi = 2.4$ and accordingly, from figure 3, $Q/G = 0.7$. Hence τ is (see (2.10))

$$\tau = \frac{a^2}{18\nu} \frac{Q(\chi)}{G(\chi)} = 0.09 \text{ s}. \tag{7.5}$$

In the actual experiment the average value of χ, estimated from photographs of the bubbly mixture, is less, about 1.8. This, apparently, is caused by the interactions.

We have measured transitions $\alpha_2 \to \alpha_1$ for a number of values of α_1 and α_2. Measurements were made both with γ-ray attenuation and with the help of electrodes, as described in §6. We shall use here α-profiles obtained with electrodes.

In figure 9 some examples are given of recordings of α when a voidage wave passes an electrode. The representation is in terms of time, which can easily be converted

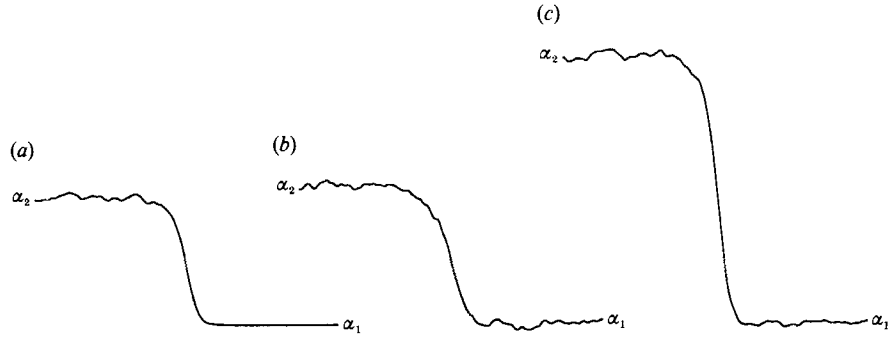

FIGURE 9. A recording of the concentration α in the transition $\alpha_2 \rightarrow \alpha_1$: (*a*) $\alpha_2 = 4.9\%$, $\alpha_1 = 0\%$; (*b*) $\alpha_2 = 15.1\%$, $\alpha_1 = 9.9\%$; (*c*) $\alpha_2 = 15.5\%$, $\alpha_1 = 5.5\%$.

to distance by using the velocity U_s of the wave. The value of U_s was always measured from two recordings a distance of 20 cm from each other. With the electrodes the recording of a concentration profile is available in the form of 2000 points, reaching from α_1 to α_2. However, many of these are in the outer regions and the number in the range where α changes rapidly is much smaller, about 200. With γ-ray attenuation there are less points in total and the number in the region of rapid change is even smaller, about 10. Because of this, we deal in the present study only with the measurements made with electrodes. Recordings of the type given in figure 9 were used to compare the measured concentration profile to the one predicted by (5.29) and (5.32). First, the shape of the transition was compared. For given values of α_1, α_2, λ and V, values of z_0 and q were determined in such a way that (5.29) fits as well as possible to the experimentally obtained recordings of α. It turned out that the shape of the α-curves obtained fits (5.29) very well. In all cases z_0 and q values are obtained such that the mean square difference between α as given by (5.29) and measured values of α is less than 3×10^{-6}. Since α is of order of 10% in our experiments this means that, with particular values of z_0 and q for each curve, the relative difference between the actual data and the prediction by (5.29) is of order of 1%. Next we compared the value of q, obtained as described above and denoted q_{exp}, with the theoretical value for q, q_{th}, given in (5.27). Together with α_2, α_1, U_s and q_{exp}, this is given in table 1 for a number of experiments.

The computation of q_{exp} from the experimental data, in the way we have just described, was done numerically. In order to have confidence in the numerical programme, an estimate for q_{exp} was obtained in another way. From the experimental data a thickness d of the transition was defined as the distance between points where α reaches $\alpha_1 + 0.05(\alpha_2 - \alpha_1)$ and $\alpha_2 - 0.05(\alpha_2 - \alpha_1)$, respectively. Since the middle part of the wave where the asymptotic expressions (5.30) and (5.31) are invalid is very short the thickness can be estimated with help of (5.32). In view of the chosen values we took the multiplicative factor preceding the expression at the right-hand side of (5.32) equal to 3 since $e^{-3} = 0.05$. Subsequently from

$$d = \frac{3\mathscr{D}}{\lambda V}\left\{\frac{\alpha_2+\alpha_1}{\alpha_2-\alpha_1} + \frac{(\alpha_1^2+\alpha_2^2)/2q}{\alpha_2-\alpha_1}\right\} \tag{7.6}$$

and using (5.28), an estimate for q_{exp}, denoted q'_{exp}, was obtained. It appears that q_{exp} and q'_{exp} are close in most cases. In figure 10 the ratio $q_{\text{exp}}/q_{\text{th}}$ is plotted against the mean concentration $\frac{1}{2}(\alpha_1 + \alpha_2)$. From this representation as well as from the data

α_2	α_1	U_s (m/s)		q_{exp}	q'_{exp}	$\mathscr{D}_{exp}$ (m^2/s)	q_{th}
		exp	theory				
0.179	0.077	0.112	0.121	0.068	0.065	0.0010	0.246
0.177	0.101	0.103	0.112	0.029	0.013	0.0004	0.257
0.155	0.055	0.128	0.140	0.110	0.115	0.0016	0.223
0.153	0.079	0.118	0.131	0.051	0.032	0.0007	0.234
0.151	0.099	0.122	0.124	0.040	0.034	0.0006	0.243
0.126	0.052	0.137	0.152	0.108	0.111	0.0016	0.207
0.126	0.026	0.151	0.162	0.188	0.185	0.0027	0.194
0.125	0.073	0.129	0.144	0.074	0.064	0.0011	0.217
0.100	0.025	0.162	0.173	0.200	0.184	0.0029	0.181
0.099	0.059	0.143	0.160	0.059	0.043	0.0008	0.197
0.097	0.047	0.149	0.166	0.093	0.071	0.0013	0.190
0.088	0.046	0.153	0.170	0.076	0.041	0.0011	0.185
0.085	0.043	0.160	0.172	0.086	0.065	0.0012	0.182
0.077	0.035	0.164	0.178	0.107	0.116	0.0015	0.174
0.073	0.021	0.176	0.186	0.192	0.171	0.0027	0.165
0.065	0.034	0.168	0.183	0.106	0.055	0.0015	0.168
0.064	0.023	0.177	0.188	0.155	0.130	0.0022	0.161

TABLE 1

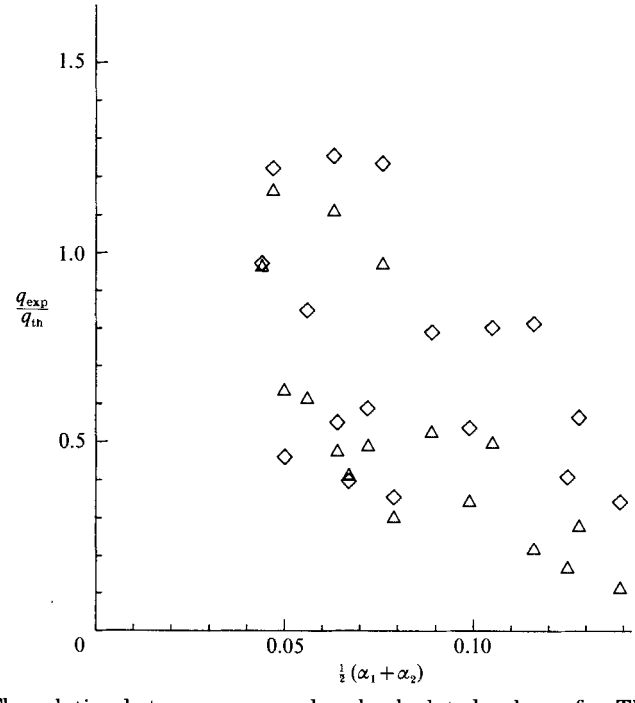

FIGURE 10. The relation between measured and calculated values of q. The points △ are q_{exp} in table 1. The points ◇ are q'_{exp}, neglecting α^2 terms in (5.32).

given in table 1 it can be seen that there is agreement as far as order of magnitude is concerned. Both q_{exp} and q_{th} are of order 10^{-1} and the corresponding diffusion coefficient $\mathscr{D}$ is of order 10^{-3} m^2/s. Inspection shows that the agreement is less with higher mean concentrations than with the lower ones. Because the theoretical

considerations are partly based on explicit results for pairs, the terms in α^2 are probably not accurate. We therefore made a second comparison of q_{th} with a value of q'_{exp} obtained by omitting in (7.6) the terms quadratic in α_1 and α_2, that is

$$d = \frac{3\mathscr{D}}{\lambda V}\frac{\alpha_2+\alpha_1}{\alpha_2-\alpha_1}. \tag{7.7}$$

These are almost the same as follow from (5.29) upon omitting the terms quadratic in α. We see that the agreement is appreciably improved. It should be observed that at higher concentrations other effects than those considered here may be important. For example, Biesheuvel & Gorissen (1989) allow viscous resistance to depend on $\partial\alpha/\partial z$ as well as on α. At low concentrations, as considered here, we think that fluid inertia is a major effect. The experiments show that the effective gradient diffusion predicted here is of the right order of magnitude and even fairly accurate at low concentrations.

8. Conclusion

In this paper the role of fluid inertia in the dynamics of voidage waves in bubbly flows is considered. While a decrease with concentration of the rise velocity of a homogeneous mixture promotes the steepening of such a wave, the increase of fluid impulse can balance this provided, roughly speaking, that the added-mass force on a bubble increases with concentration more than the viscous resistance does. For sufficiently slow gradients of α the transition profile in voidage waves can be predicted solely from data on the uniform velocity of rise. Experiments show that there is order-of-magnitude agreement with such predictions for all experiments done by us and numerical agreement up to concentrations of about 8%.

With great pleasure we dedicate this paper to George Batchelor on the occasion of his 70th birthday. His work has been for almost half a century a source of inspiration for workers in fluid mechanics, especially over the last decades for those engaged in research in heterogeneous media. One of us (L. v. W.) adds to this his appreciation and gratitude for a longstanding friendship and cooperation.

The authors thank A. Biesheuvel and W. C. M. Gorissen for fruitful discussions and help during the preparation of this paper. Thanks are due to the referees for their useful comments and criticisms. This research was supported by Fundamenteel Onderzoek der Materie (FOM) under contract no. 280213.

Appendix A

Consider two oblate spheroids with their line of centres normal to the parallel short axes (see figure 11). With velocity $\dot{x}$ in the direction of $\boldsymbol{e}_1$, let the dipole strength be $\beta\dot{x}\mathscr{V}$ for each of the spheroids in the absence of the other. Spheroid 2 will, when they form a pair, induce in the centre of spheroid 1 a velocity u_{ind}. Then, in an approximation accurate to $(a/R)^3$, where a is the effective radius of a spheroid and $2R$ the distance separating the centres, the dipole strength is $\beta_1\dot{x}\mathscr{V}(1-u_{\text{ind}}/\dot{x})$. This dipole in turn induces in the centre of spheroid 2 a velocity

$$\frac{2\dot{x}}{(2R)^3}\beta_1\mathscr{V}\left(1-\frac{u_{\text{ind}}}{\dot{x}}\right), \tag{A 1}$$

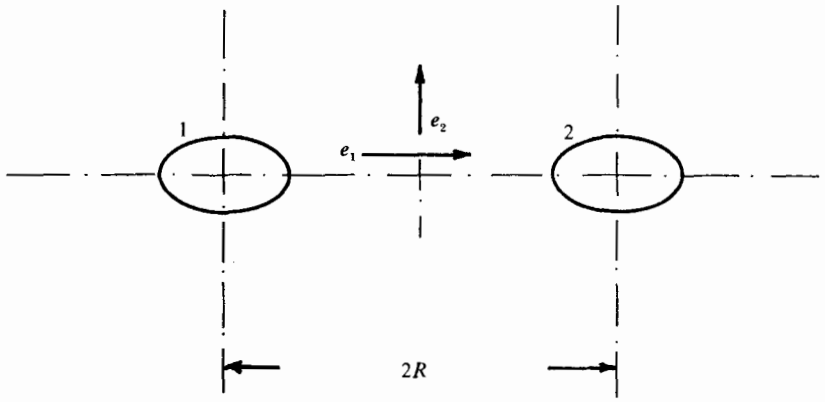

FIGURE 11. Two oblate spheroids with effective radius a and separated by a distance $2R$.

which is, by symmetry, just equal to u_{ind}, whence

$$\frac{u_{\text{ind}}}{\dot{x}} = \frac{2}{(2R)^3}\beta_1 \mathscr{V} + O\left(\frac{a}{R}\right)^4. \tag{A 2}$$

From (3.5) and the discussion following (3.12) in §3 on the relation between drag force and dissipation, we have

$$(\boldsymbol{F}\cdot\boldsymbol{e}_1)\cdot\boldsymbol{e}_1 = -2u_{\text{ind}}/\dot{x} = -4\beta_1 \mathscr{V}/(2R)^3, \tag{A 3}$$

where the second equality has been obtained with use of (A 2). Writing for the impulse $\boldsymbol{h}$

$$\boldsymbol{h} = \boldsymbol{M}\cdot(\boldsymbol{I}+\boldsymbol{L})\cdot\boldsymbol{x},$$

(3.7) gives for the aligned case

$$M_{11}\dot{x}\{1+(\boldsymbol{L}\cdot\boldsymbol{e}_1)\cdot\boldsymbol{e}_1\} = 4\pi\rho_\ell \mathscr{V}\beta_1\dot{x}(1-u_{\text{ind}}/\dot{x}) - \rho_\ell \mathscr{V}\dot{x}.$$

Using (A 2) for $u_{\text{ind}}/\dot{x}$ gives

$$M_{11}\{1+(\boldsymbol{L}\cdot\boldsymbol{e}_1)\cdot\boldsymbol{e}_1\} = 4\pi\rho_1\beta_1 \mathscr{V}(1-2\beta_1 \mathscr{V}/(2R)^3) - \rho_\ell \mathscr{V}. \tag{A 4}$$

Letting R become infinite gives

$$M_{11} = 4\pi\rho_\ell\beta_1 \mathscr{V} - \rho_\ell \mathscr{V}.$$

Using this in (A 4) gives, together with (A 3),

$$(\boldsymbol{L}\cdot\boldsymbol{e}_1)\cdot\boldsymbol{e}_1 = \frac{1}{2}\left(1+\frac{\rho_\ell \mathscr{V}}{M_{11}}\right)(\boldsymbol{F}\cdot\boldsymbol{e}_1)\cdot\boldsymbol{e}_1. \tag{A 5}$$

This result is mentioned in the main text. In the case of motion in the $\boldsymbol{e}_2$ direction a similar result is found. The relation (A 1) becomes

$$\frac{\dot{x}}{(2R)^3}\beta_2 \mathscr{V}\left(1+\frac{u_{\text{ind}}}{\dot{x}}\right),$$

and M_{22} must be used instead of M_{11}. As observed in the main text M_{22} is given by (2.8) while M_{11} is given in Lamb (1932, §373).

Appendix B

In §6 it was reported that the electrodes respond to a stepwise variation of the concentration $\mathrm{d}\alpha/\mathrm{d}x = \Delta\alpha\,\delta(x)$ with

$$\alpha_e = \tfrac{1}{2}\Delta\alpha\{1+\tanh sx\}, \quad s = 115\ \mathrm{m}^{-1}.$$

We now investigate the response to a wave-like change

$$\frac{\mathrm{d}\alpha}{\mathrm{d}x} = \frac{\lambda\Delta\alpha}{2\cosh^2\lambda x}, \quad \lambda < s.$$

This gives for the signal α_e of the electrodes

$$\begin{aligned}\alpha_e &= \tfrac{1}{4}\Delta\alpha\lambda\int_{-\infty}^{\infty}\frac{1+\tanh s(x-\xi)}{\cosh^2\lambda\xi}\mathrm{d}\xi = \tfrac{1}{2}\Delta\alpha+\tfrac{1}{4}\Delta\alpha\int_{-\infty}^{\infty}\frac{\lambda\tanh s(x-\xi)}{\cosh^2\lambda\xi}\mathrm{d}\xi\\ &= \tfrac{1}{2}\Delta\alpha+\tfrac{1}{4}\Delta\alpha\int_{-\infty}^{\infty}\frac{s\tanh\lambda(x-\xi)}{\cosh^2 s\xi}\mathrm{d}\xi\\ &= \tfrac{1}{2}\Delta\alpha\left\{1+\frac{1}{2}\int_{-\infty}^{\infty}\frac{\tanh\lambda x-\tanh\lambda\rho/s}{\cosh^2\rho(1-\tanh\lambda x\tanh\lambda\rho/s)}\mathrm{d}\rho\right\}.\end{aligned}$$

For values of x such that $\tanh\lambda x \sim 1$, the integral equals 2, so that the width of the wave is not affected. For values of x for which $|\tanh\lambda x| < 1$, we write

$$\begin{aligned}\alpha_e &= \tfrac{1}{2}\Delta\alpha(1+\tanh\lambda x)-\frac{\tfrac{1}{4}\Delta\alpha\tanh\lambda x}{\cosh^2\lambda x}\int_{-\infty}^{\infty}\frac{\tanh\lambda\rho/s}{\cosh^2\rho(1-\tanh\lambda x\tanh\lambda\rho/s)}\mathrm{d}\rho\\ &\approx \tfrac{1}{2}\Delta\alpha\left[1+\tanh\lambda x\left\{1-\frac{1}{2\cosh^2\lambda x}\int_{-\infty}^{\infty}\frac{(\tanh\lambda\rho/s)^2}{\cosh^2\rho}\mathrm{d}\rho\right\}\right].\end{aligned}$$

The integral is of order $(\lambda/s)^2$ for small λ/s and has the value $\frac{2}{3}$ for $\lambda = s$, so that a good estimate is

$$\alpha_e \approx \tfrac{1}{2}\Delta\alpha\left[1+\tanh\lambda x\left\{1-\frac{(\lambda/s)^2}{3\cosh^2\lambda x}\right\}\right].$$

With $\lambda/s \leqslant 0.5$, this means a maximum relative error (near $x = 0$) of about 8%.

REFERENCES

Batchelor, G. K. 1972 Sedimentation in a dilute dispersion of spheres. *J. Fluid Mech.* **52**, 245–268.

Batchelor, G. K. 1988 A new theory of the instability of a uniform fluidized bed. *J. Fluid Mech.* **193**, 75–110.

Batchelor, G. K. 1989 A brief guide to two-phase flow. In *Theoretical and Applied Mechanics* (ed. P. Germain, M. Piau & D. Cailleric), pp. 27–39. North-Holland.

Biesheuvel, A. 1984 On void fraction waves in dilute mixtures of liquid and gas bubbles. Ph.D. thesis, University of Twente.

Biesheuvel, A. & Gorissen, W. C. M. 1990 Void fraction disturbances in a uniform bubbly fluid. *Intl J. Multiphase Flow* (to appear).

Biesheuvel, A. & Wijngaarden, L. van 1982 The motion of pairs of gas bubbles in a perfect fluid. *J. Engng Maths* **16**, 349–365.

Bouré, J. 1988 Properties of kinematic waves in two phase pipe flows. Presented at European Two-Phase Flow Group Meeting, Brussels, 30 May–1 June.

Chapman, S. & Cowling, T. G. 1939 *The Mathematical Theory of Nonuniform Gases*. Cambridge University Press.

CLIFT, R., GRACE, J. R. & WEBER, M. E. 1978 *Bubbles, Drops and Particles.* Academic.

KOK, J. B. W. 1988 Hydrodynamic equations and effective properties of bubbly flows. In *Transient Phenomena in Multiphase Flow* (ed. N. Afgan), pp. 127–136. Hemisphere.

KOK, J. B. W. 1989 Dynamics of gas bubbles moving through liquid. Thesis, University of Twente.

LAMB, H. 1932 *Hydrodynamics.* Dover.

LIGHTHILL, M. J. 1986 *An Informal Introduction to Theoretical Fluid Mechanics.* Oxford University Press.

MILNE THOMSON, L. M. 1968 *Theoretical Hydrodynamics.* Macmillan.

MOORE, D. W. 1963 The boundary layer on a spherical gas bubble. *J. Fluid Mech.* **16**, 161–176.

MOORE, D. W. 1965 The velocity of rise of distorted gas bubbles in a liquid of small viscosity. *J. Fluid Mech.* **23**, 749–766.

RYSKIN, G. & LEAL, L. G. 1984 Numerical solution of free-boundary problems. Part 2. Buoyancy-driven motion of a gas bubble through a quiescent liquid. *J. Fluid Mech.* **148**, 19–35.

WIJNGAARDEN, L. VAN 1976 Hydrodynamic interaction between gas bubbles in liquid. *J. Fluid Mech.* **77**, 27–44.

WIJNGAARDEN, L. VAN & BIESHEUVEL, A. 1988 Voidage waves in mixtures of liquid and gas bubbles. In *Transient Phenomena in Multiphase Flow* (ed. N. Afgan), pp. 275–289. Hemisphere.